Int. J. Electrochem. Sci., 12 **(2017)** 8269 – 8279, doi: 10.20964/2017.09.46

International Journal of ELECTROCHEMICAL SCIENCE
www.electrochemsci.org

Short Communication

Corrosion Behavior Study of AZ31B magnesium Alloy by Sol-Gel Silica-based Hybrid Coating

Zhiqiang Qian [1,2,3], *Shidong Wang* [1,2,*], *Zhijian Wu* [1,2,*]

[1] Key Laboratory of Comprehensive and High Efficient Utilization of Salt Lake Resources, Qinghai Institute of Salt Lakes, Chinese Academy of Sciences, Xining 810008, China
[2] Key Laboratory of Salt Lake Resources Chemistry of Qinghai Province, Qinghai Institute of Salt Lakes, Chinese Academy of Sciences, Xining 810008, China
[3] University of Chinese Academy of Sciences, Beijing 100049, China
[*]E-mail: wshidong1006@163.com, zjwu@isl.ac.cn

Received: 7 June 2017 / *Accepted:* 14 July 2017 / *Published:* 13 August 2017

In this work, the silica-based hybrid coatings, which used 3-glycidoxypropyltrimethoxysilane (GPTMS) and tetraethoxysilane (TEOS) as precursors, have been prepared by sol–gel method for protection of magnesium alloy (AZ31B) from corrosion. The morphology and surface chemistry of the optimized coatings were studied by scanning electron microscope (SEM) and Fourier transform infrared (FTIR), respectively. The corrosion behaviors of the coatings were evaluated by polarization curves measurements and electrochemical impedance spectroscopy (EIS) in the Harrison's solution (0.35wt% $(NH4)_2SO_4$ + 0.05wt% NaCl), and the diagrams were fitted using equivalent electrical circuits (EEC). The results revealed that the compact and smooth hybrid silane films were formed on the substrates surface, which provided barrier protection and improved corrosion resistance ability in comparison to untreated magnesium alloy substrate.

Keywords: AZ31B magnesium alloy; Sol-gel; Corrosion protection; Electrochemical impedance spectroscopy (EIS)

1. INTRODUCTION

Magnesium and its alloys have drawn high attention by using as lightweight structural materials for automobiles, aircrafts, electronic products owing to their low density, good consistency, high specific strength, etc. [1-2]. However, the presence of bimetallic phases at the grain boundaries limited their larger scale applications because of the poor corrosion resistance and high chemical reactivity. Corrosion of magnesium alloy is mainly caused by chemical or electrochemical reaction

between magnesium alloy and the surrounding medium, such as moist air, water and electrolyte. Therefore, it is necessary to design an effective anticorrosion coating on magnesium alloy surface, which make magnesium alloy isolated from the corrosive medium, and enhanced the corrosion resistance of magnesium alloys. In order to alleviate the aggressive corrosion of the magnesium alloys, many techniques have been investigated, such as chemical conversion [3,4], sol-gel coating [5,6], anodization [7,8], electrodeposition [9,10], etc. Among these methods, the sol–gel organic–inorganic hybrid coating provides a simple, low cost, non-hazardous method for preparing coatings with controllable composition, microstructure and functional properties.

The sol-gel organic–inorganic hybrid coatings, which are formed via hydrolysis and condensation reactions between organically modified silanes and inorganic silica precursors to get good adhesion between the surface and the coating by stable covalent bonds, have been widely applied on various metal substrates [11-16]. In recent years, the sol–gel hybrid coatings on magnesium alloys have been reported. Guo [17] prepared a sol coated on the AZ31B alloy substrate via self-assembled nanophase particle (SNAP) technology. This SNAP film was synthesized by the organosilanes of 3-glycidoxypropyltrimethoxysilane (GPTMS) and tetraethoxysilane (TEOS), and the crosslink agent (triethylene tetramine (TETA)), formed a silica network, which increased the thermal stability, compactness and corrosion protection. Peres [18] prepared a GPTMS-TEOS based hybrid coating on AZ31B alloys, indicated the addition of SiO_2 nanoparticles into the hybrid coating improved the electrochemical response of the system and seemed to retard the corrosion process. The introduction of earth-ion into silane hybrid coatings were also studied by Qiao [19] and Zhong [20], the results showed that they could increase film thickness and hydrophobicity, and improve the anti-corrosion behavior.

In the present work, the sol–gel derived GPTMS–TEOS hybrid coatings have been prepared on AZ31B alloys surface via a dip-coating procedure, which revealed superior corrosion property compared with the bare alloy substrates. The fabricated coatings are characterized using Fourier transform infrared (FT-IR) and scanning electron microscopy (SEM) techniques. A comprehensive study of EIS feature of the coatings during immersion in Harrison solution was investigated, and electrical equivalent circuits (EEC) were simulated according to the experimental data.

2. EXPERIMENTAL

2.1. Materials

The AZ31B Mg alloy was obtained from Dongguan hongxing metal materials co., LTD. The dimension of the AZ31B samples used for the experiments was 60 mm × 40 mm × 3 mm. Tetraethoxysilane (TEOS, 98%), 3-glycidoxypropyltrimethoxysilane (GPTMS, 97%), triethylene tetramine (TETA, 97%), and acetic acid (CH_3COOH, 98%) were analytical pure and purchased from Sinopharm Chemical Reagent Co. Ltd.

2.2. Preparation of the sol-gel silica-based hybrid coating

Firstly, the AZ31B plate samples were polished using 320, 800, and 2000 grit silicon carbide waterproof abrasive papers in turn. After polishing, the plate samples were ultrasonically cleaned in ethanol and water, respectively, and dried with a hairdryer.

Then, the hybrid sol-gel was prepared as following: 11 ml TEOS and 33.8 ml GPTMS were added in 18 ml 0.05 mol·L^{-1} dilute acetic acid under stirring at room temperature for 3 h. After aging for 4 days to ensure complete hydrolysis, the crosslink agent of 0.75 mL TETA was added into the sol under stirring at room temperature for 5 min. The hydrolysis reactions for the preparation can be illustrated as Scheme1.

Finally, the hybrid sol-gel coatings of AZ31B alloy were produced through a dip-coating procedure conducted by immersion of the prepared specimens in the sol for 3 min, followed by controlled withdrawal rate of 1 mm/s. After coating application, the specimens were cured at 100˚C in oven for 30 min.

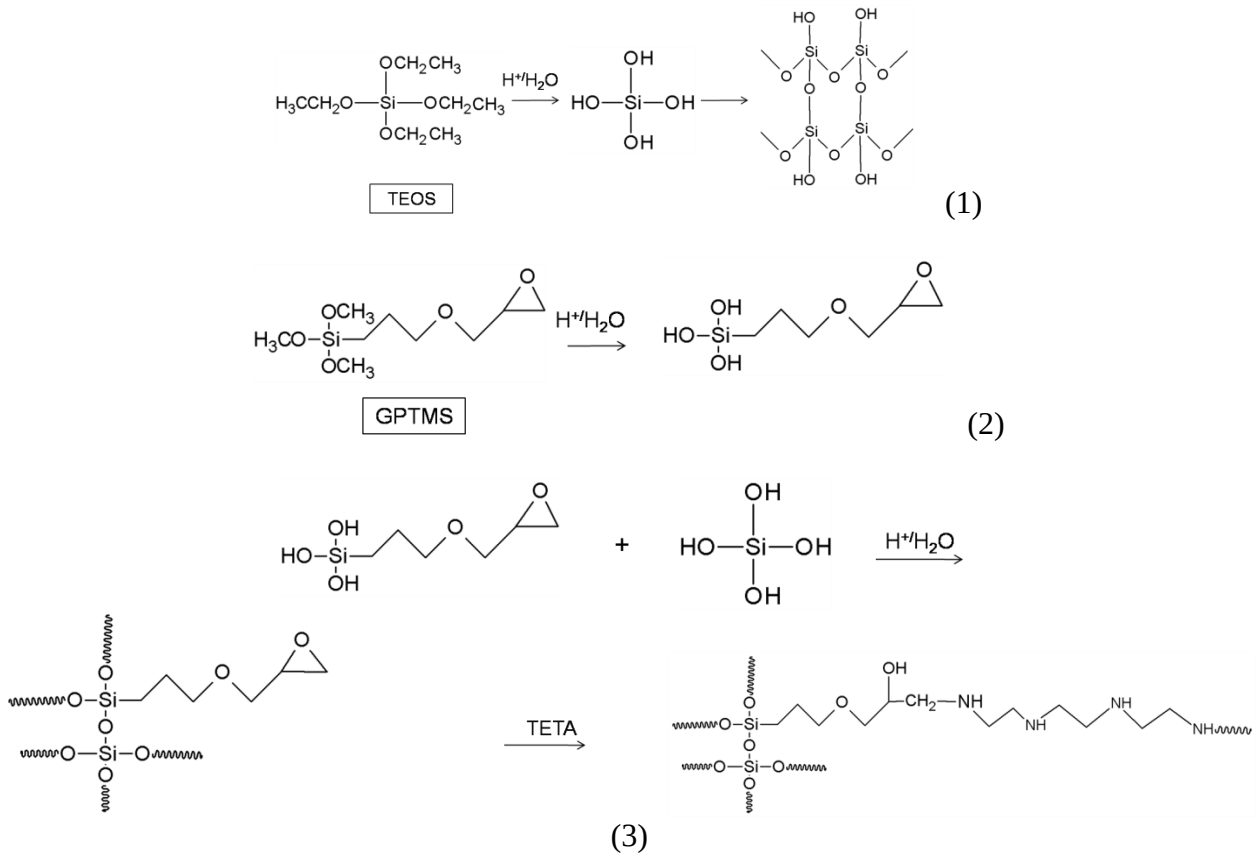

Scheme 1. The hydrolysis process of silane sol–gel coating

2.3. Characterization and tests

Field emission scanning electron microscopy (FESEM) investigations were performed using a Hitachi SU8010 FESEM. Fourier transform infrared (FTIR) spectra were obtained by a Nexus

instrument from Thermo Nicollet, USA. The measurement parameters were set as a wavenumber range from 4000 to 650 cm^{-1} with a resolution of 4 cm^{-1}.

All electrochemical measurements were conducted on a CHI604E electrochemical workstation (Shanghai Chenghua Instrument Co., Ltd, China) using a standard three-electrode system at room temperature, in which a platinum plate as the auxiliary electrode, a saturated calomel electrode (SCE) as the reference electrode, and the sample to be tested as the test electrode. The exposure area of the tested sample was 1 cm^2. Polarization curves were obtained in 3.5 wt% NaCl solutions within a potential range of open circuit potential (OCP) ±250 mV at a scan rate of 1 mV s^{-1}. The corrosion current (I_{corr}), potential (E_{corr}), and Tafel slopes were determined using an extrapolation method [21]. The electrochemical impedance spectra (EIS) were carried out in Harrison solution (0.35wt% $(NH4)_2SO_4$ + 0.05wt% NaCl). The measuring frequency of EIS ranged from 10^5 Hz to 10^{-2} Hz with the perturbation potential of 5 mv at the open circuit potential. During the EIS test, the sample was exposed to the Harrison solution, and after a certain period of time, the test was carried out and the impedance value was record. The EIS spectra were fitted using the ZSimpWin software. All the samples were immersed in the test medium for 30 min before the date was obtained.

3. RESULTS AND DISCUSSION

3.1. Characterization of the hybrid coating

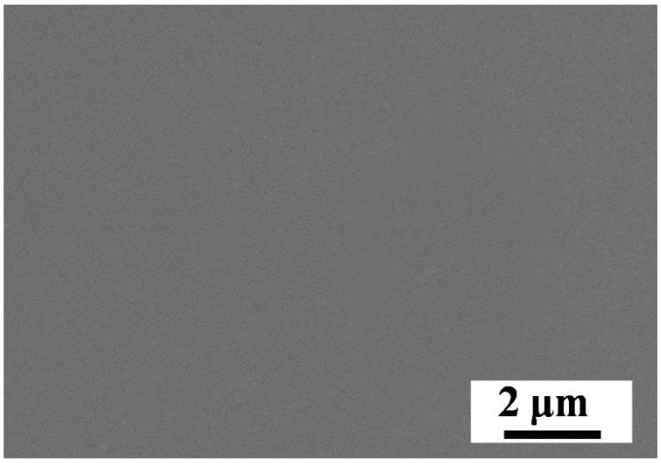

Figure 1. Surface morphology of the hybrid coating

The surface morphology of the hybrid coating is assessed by FESEM. As shown in Fig. 1, a homogeneous and smooth thick coating is obtained by sol–gel process. The crack-free thick coatings can be formed due to the crosslink reaction by the precursor molecules and the organic crosslink agent, acting as a physical barrier by impeding intrusion of water and electrolyte into the metallic substrate, which improve the corrosion resistance of the substrate [22].

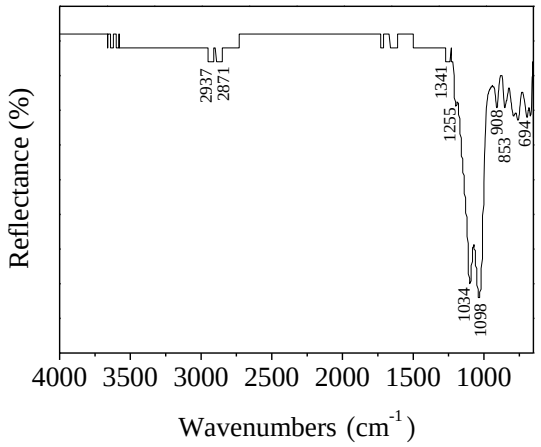

Figure 2. FT-IR of the hybrid coating

The FTIR spectrum of the hybrid coating is given in Fig. 2. The characteristic bonds at 908 cm^{-1} attributed to vibration of epoxy functional groups form GPTMS [22]. As expected, the asymmetric Si-O-Si stretching vibration characteristic of siloxane network formation being evidence condensation reaction between adjacent silanol groups is observed at 1034 and 1098 cm^{-1}, while the peak at 853 cm^{-1} can be attributed to symmetric Si-O-Si bond stretching vibration [23]. The absorption bands around 2937 and 2871 cm^{-1} are attributed to stretching vibrations of C-H bonds in $-CH_3$ and $-CH_2$, respectively [24]. The bands around 1341 and 1255 cm^{-1} are attributed to the asymmetric and symmetric stretching vibrations of C-O and C-O-C bonds [23]. The bonds lying at 694 cm^{-1} is attributed to Si-O-Mg [24], which indicates that the film was successfully bonded to the surface of AZ31B alloy. According to the results, it can be inferred that the hydrolysis reaction of GPTMS and TEOS produces the cyclic siloxane ring structure nanoparticle with epoxy functional groups, which may be capable of reacting with Mg substrate forming an interface with a higher density of Mg-O-Si bonds.

3.2. Corrosion behaviors of the hybrid coatings

In order to estimate the ability of the hybrid coatings for corrosion protection on the AZ31B alloy surface, potentiodynamic polarization and electrochemical impedance spectroscopy (EIS) measurements were carried out using an electrochemical workstation. Fig. 3 shows potentiodynamic polarization curves of the bare alloy and the hybrid coating after immersion in 3.5 wt% NaCl for 30 min. Corrosion potential (E_{corr}), corrosion current density (I_{corr}), and Tafel constants of β_a and β_c, were derived based on the polarization curves, and the parameters of the potentiodynamic polarization are listed in Table 1. Compared with the bare AZ31B alloy, the corrosion current density I_{corr} of the hybrid coating decreases a more than three-order of magnitude, reflecting the improvement in corrosion protection.

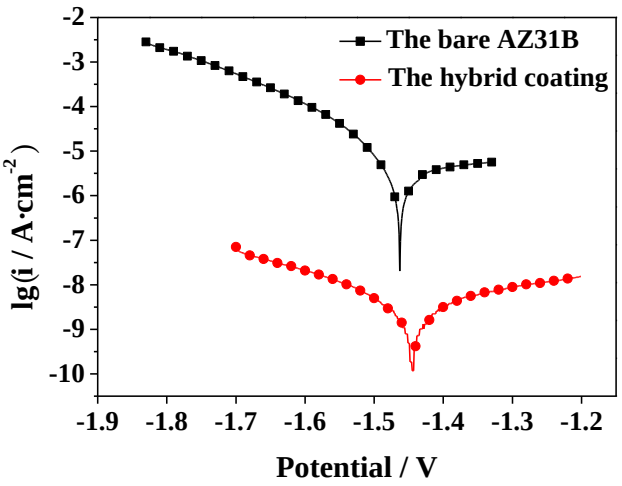

Figure 3. Potentiodynamic polarization curves of bare alloy and the hybrid coating in 3.5 wt% NaCl solution

Table 1. Corrosion potential (Ecorr) and corrosion current density (Icorr) of the bare alloy and the hybrid coating

	Ecorr (V)	*Icorr* (μA/cm^2)	*βc* (mV/dec)	*βa* (mV/dec)
Bare sample	-1.463	4.195	94.67	833.75
Coated sample	-1.445	3.681E-3	150.85	243.61

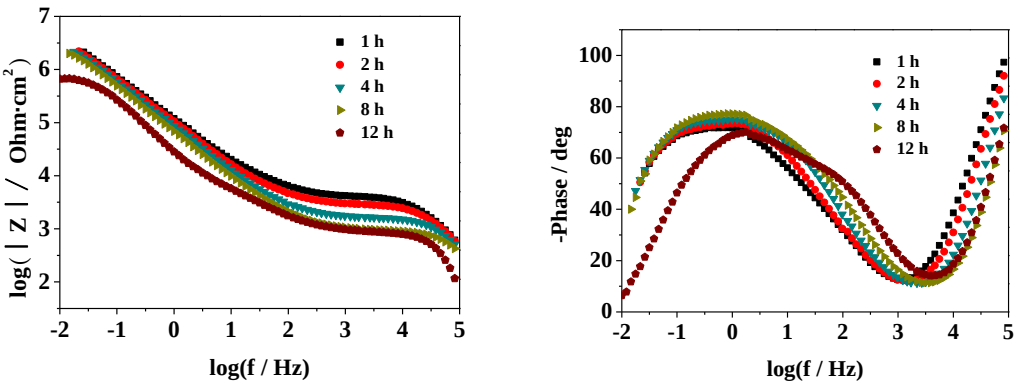

Figure 4. EIS plots obtained for the coated AZ31B alloy at primary stage of immersion (1h-12h) in Harrison's solution

As is known to all, the electrochemical impedance spectroscopy (EIS) is one of the most efficient and intensive technique for investigation of the corrosion behaviors and the coating degradation in solution corrosion medium [25]. The degradation of the sol-gel coating can be assessed by low frequency impedance values (LF, 0.01 Hz) and the emergence of new time constants [24]. In

this section, EIS was estimated the anticorrosion behaviors and degradation of the hybrid coatings in Harrison solution. The changes of the impedance spectra with immersion time of sol-gel coating were presented in Figs. 4-5.

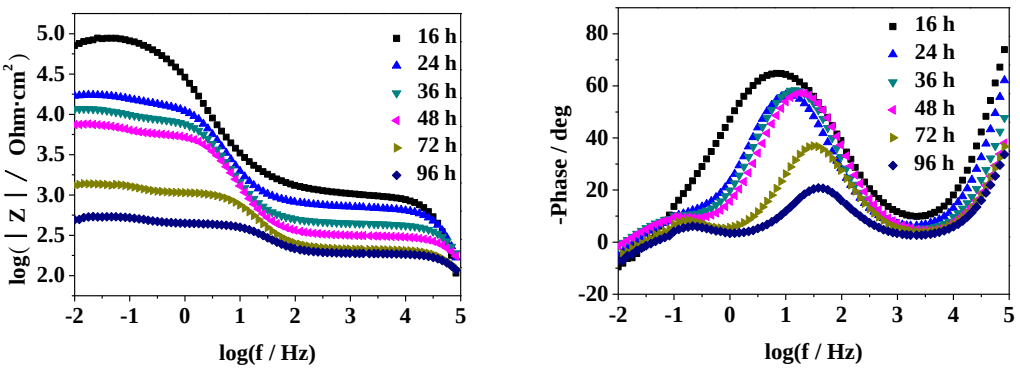

Figure 5. EIS plots obtained for the coated AZ31B alloy at later stage of immersion (16h-96h) in Harrison's solution

It can be inferred that the hybrid coatings maybe consist of three areas from outside to inside: the outer layer is a film crosslinked by Si-O-Si bond; the interface layer is between metal and film caused by Si-O-Mg and Si-O-Si bonds; the inside is the responses of charge transfer process and the electric double layer on the surface of the metal substrates [26-27].

Fig. 4 presents the EIS spectra with immersion time from 1 h to 12 h. In this immersion stage, it presents two time constants, one is reflection of film properties including resistance and capacitance at high frequency, the other is metal/film interface reflection at low frequency. In the initial period of immersion, it can be seen that the impedance value at LF decreases slowly with time. At this stage, as the film is hydrophobic, it is impregnated with electrolyte while the natural MgO layer still remained intact. After immerse in the electrolyte more than 12 h, the impedance value reveals a marked decrease. The increase of the immersion time leads to the decrease of the impedance value at LF, suggesting the gradual degradation of the coating. Then, the shape of these spectra changed and revealed three time constants after 16 h immersion. Moreover, the spectra revealed a well-defined low frequency inductive loop, which was attributed to the corrosion nucleation at the surface of silane film [19]. This period can be considered as the primary stage of corrosion. The EIS spectra with immersion time from 16 h to 96 h were presented in Fig. 5.

In order to evaluate barrier performance and degradation of the sol-gel coating in the corrosion process, the EIS spectra were fitted by equivalent circuit. Due to the deviation of the capacitance in the EEC with pure capacitor, constant phase angle element (*CPE*) is used to replace the pure capacitor. The capacitance is calculated using the following formula [28]:

$$C = Q(\omega_{max})^{n-1} \quad (4)$$

where, ω_{max} represents the frequency at which the imaginary part of impedance reaches a maximum. n represents the correlation coefficient ($0 < n \leq 1$) and Q is the symbol of *CPE*.

Fig. 6 shows the EECs used in the experiment. In these circuits, *R*s represents the resistance of the electrolyte. R_c and CPE_c represent the resistance and capacitance associated with the silane film, respectively. R_{ox} and CPE_{ox} represent the resistance and capacitance of interlayer between silane film and substrate. R_{ct} and CPE_{dl} represent the resistance and capacitance of the charge transfer process and the response of electric double layer on the alloy substrate, which are often observed when corrosion starts on the metal substrate under the coating. The experimental spectra were fitted by equivalent circuit with high fitting degree, and the parameters were obtained. The fitted values were presented in Table 2.

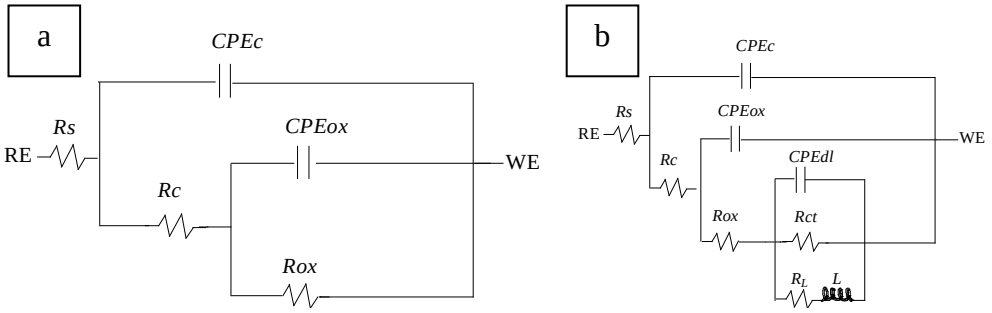

Figure 6. Equivalent circuits used for numerical simulation of the EIS plots (a) Primary stage of immersion; (b) Later stage of immersion

The parameters revolution was analyzed to evaluate the corrosion protection performance of the coating system. The values of the elements in the circuit can provide information concerning water uptake in the coating, change in the resistive properties of the coating, development of the coatings delimitation and initiation and propagation of corrosion at the metal/coating interface.

Table 2. Parameters of the sol–gel film/substrate systems obtained from fitting of the experimental impedance spectra with equivalent circuit at primary stage of immersion

t (h)	CPE_c ($F \cdot cm^{-2}$)	R_c ($ohm \cdot cm^2$)	CPE_{ox} ($F \cdot cm^{-2}$)	R_{ox} ($ohm \cdot cm^2$)
1	3.019E-9	4204	1.932E-6	1.035E7
2	3.187E-9	3008	2.119E-6	6.9E6
4	3.688E-9	1711	2.463E-6	5.287E6
8	5.435E-9	1006	2.956E-6	4.109E6
12	4.811E-9	889.2	2.892E-6	8.292E5
16	4.709E-9	1043	1.579E-6	1.18E4
24	6.17E-9	704.1	7.295E-6	1.359E4
36	5.776E-9	413.6	8.622E-6	8612
48	8.954E-9	257.1	6.426E-6	5301
72	2.016E-8	200.8	2.049E-5	876.7
96	1.234E-8	151.9	2.344E-5	244.6

As electrolyte has smaller resistance and larger capacitance constant, its infiltration will change the coating resistance and capacitance. Generally speaking, the dielectric layer capacitance depends on the absorption amount of electrolyte. With the extension of immersion time, the film capacitance increased gradually. Resistance, another important parameter of the film, with the extension of immersion time, it was reduced due to penetration of the electrolyte ions in the solution. The outer film was crosslinked by Si-O-Si bond, but it was not stable in the aqueous solution [1]. It slowly hydrolyzed to Si-OH groups, lowered the crosslinking density of the film and the film became thinner. In turn, the resistance of the film reduced. The decrease of the film capacitance after immersion for 12h may due to the thinning of the film, which was caused by the dissolution of the film. For the same reason, a sudden decrease can be seen after 96h immersion. However, at the start of immersion (1h), as the coating is relatively thick, *Rc* is small (about 4204 ohm·cm^2), indicating that it does not effectively hinder electrolyte access to the metallic surface.

From the point of corrosion protection, the density of interface oxide layer between film and metal substrate is very important. Due to the breakdown of interface layer, it can lead to corrosion agents directly intrude into the surface of the metal substrate. At the start of immersion (1h), the value of *Rox* is very bigger (about 1.035E7 ohm·cm^2) compared to *Rc*. Even after 12h immersion, it still remains high (about 8.292E5 ohm·cm^2). Then *Rox* dramatically falls for more long time immersion, indicating that the barrier properties of the coating are rather poor. Although the corrosion protection performance of the coating was closely related to the formation of Me-O-Si bond, but it was not stable in the aqueous solution. When exposed in aqueous solution, Me-O-Si bond hydrolyzed back to Me-OH and Si-OH groups. Compared to Si-O-Si bond in the outer film, Me-O-Si bond had higher ionic character and it lead to the attack of the polar water molecules. Me-O-Si bond can be hydrolyzed more rapidly [20]. With the hydrolysis of covalent bond, the adhesion strength of the interface layer was greatly reduced and leading to the anti-corrosion performance was lost gradually.

The rate of the corrosion processes can be estimated by measuring the polarization resistance. The polarization resistance for the coated alloy is large (about 6.169E4 ohm·cm^2) at 16h and fast decreases with immersion time. The capacitance of electric double layer gradually increased with immersion time due to the increase of corrosion product.

The above results demonstrate the degradation process of the sol-gel coating during immersion. The chemical structure changes of the coating during immersion were successfully interpreted by the evolution of the system parameters. The sol-gel coating combined with the substrate via the covalent bonds, which made AZ31B alloy isolated from the corrosive medium. However, the covalent bond hydrolyzed due to the prolongation of the immersion time in the electrolyte, which gradually reduced the corrosion resistance of the coating.

4. CONCLUSIONS

In summary, the sol-gel derived silica-based hybrid coating was fabricated on AZ31B alloy via a dip-coating procedure. The corrosion mitigation ability of the coatings was investigated by electrochemical impedance spectroscopy (EIS) and potentiodynamic polarization (PP) analyses. In

contrast to bare AZ31B alloy, the i_{corr} decreased by about three orders of magnitude immersed in 3.5 wt% NaCl aqueous solution, which was clearly testified the excellent anti-corrosion of the coating. By EIS analysis, the changes of coating chemical structure with different immersion time were obviously reflected by the evolution of the system parameters. The covalent bond formed in the coating played a vital role in barrier performance; however the stability of the bond itself in the solution is weak. The covalent bond hydrolyzed with the prolongation of the immersion time in the electrolyte, which reduced the barrier performance of coating and the corrosion process of magnesium alloy occurred.

References

1. R. G. Hu, S. Zhang, J. F. Bu, C.J. Lin and G.L. Song, *Prog. Org. Coat.*, 73 (2012) 129.
2. J.E. Gray and B. Luan, *J. Alloy. Compd.*, 336 (2002) 88.
3. H. Tang, T. Wu, F.J. Xu, W. Tao and J. Xian, *Int. J. Electrochem. Sci.*, 12 (2017) 1377.
4. H. Zhang, R. Luo, W. Li, J. Wang, M.F. Maitz, J. Wang, G. Wan, Y. Chen, H. Sun, C. Jiang, R. Shen and N. Huang, *Corros. Sci.*, 94 (2015) 304.
5. A. N. Khramov and J. A. Johnson, *Prog. Org. Coat.*, 65 (2009) 381.
6. F. Brusciotti, D.V. Snihirova, H. Xue, M.F. Montemor, S.V. Lamaka and M. G. S. Ferreira, *Corros. Sci.*, 67 (2013) 82.
7. X. J. Cui, X. Z. Lin, C. H. Liu, R. S. Yang and X.W. Zheng, *Corros. Sci.*, 90 (2015) 402.
8. T. Ishizaki, J. Hieda, N. Saito, N. Saito and O. Takai, *Electrochimi. Acta*., 55 (2010) 7094.
9. J. L. Zhang, C. D. Gu, Y. Y. Tong, W. Yan and J. P. Tu, *Adv. Mater. Interfaces*, 3 (2016) 1500694.
10. B. J. Han, Y. Yang, L. Fang, G. H. Peng and C. B. Yang, *Int. J. Electrochem. Sci.*, 12 (2017) 1377.
11. K. A. Yasakau, M. L. Zheludkevich, O. V. Karavai, and M. G. S Ferreira, *Prog. Org. Coat.*, 63 (2008), 352.
12. K. A. Manjumol, L. Mini, A. P. Mohamed, U. S. Hareesh and K.G. K. Warrier, *RSC. Adv.* 3 (2013) 18062.
13. D. Wang and G.P. Bierwagen, *Prog. Org. Coat.* 64 (2009) 327.
14. H. Rahimi, R. Mozafarinia, R. S. H. Razavi, E. Paimozd and A. Hojjati Najafabadi, *Adv. Mater. Res.* 239 (2011) 736.
15. D. Raps, T. Hack, J. Wehr, M.L. Zheludkevich, A.C. Bastos, M.G.S. Ferreira, and O. Nuyken, *Corros. Sci.* 51 (2009) 1012.
16. H. Rahimi, R. Mozaffarinia and A. H. Najafabadi, *J. Mater. Sci. Technol*, 29 (2013), 603.
17. X. H. Guo, M. Z. An, P. X. Yang, C. N. Su and Y. H. Zhou , *J Sol-Gel Sci Technol*, 52 (2009) 335.
18. R. N. Peres, E. S. F. Cardoso, M. F. Montemor, H. G. de Melo, A. V. Benedetti and P. H. Suegama, *Surf Coat Tech*, 303 (2016) 372.
19. Y. J. Qiao, W. P. Li, G. X. Wnag and X. H. Zhang, *J Rare Earth*, 33 (2015) 647.
20. X. K. Zhong, Q. Li, J. Y. Hu, X. K. Yang, F. Luo and Y. Dai, *Prog. Org. Coat.*, 69 (2010) 52.
21. E. Ozkan, C. C. Crick, A. Taylor, E. Allan and I. P. Parkin, *Chem. Sci.* 8 (2016) . 5126.
22. R.V. Lakshmi, G. Yoganandan, K.T. Kavya and B. J. Basu, *Prog. Org. Coat.*, 76 (2013) 367.
23. P. Balan, R. K. Singh Raman, ES. Chan, M.K. Harun and V. Swamy, *Prog. Org. Coat.*, 90 (2016) 222.
24. K. H. Wu, M. C. Li, C. C. Yang and G. P. Wang, *J Non-cryst Solids*, 352 (2006) 2897.
25. G. S. Popkirov, E. Barsoukov, R. N. Schindler, *J Electroanal Chem*, 425 (1997) 209.
26. M. L. Zheludkevich, R. Serra, M. F. Montemor, K. A. Yasakau, I. M. Miranda Salvado and M. G. S. Ferreira, *Electrochimi Acta*, 51 (2005) 208.
27. W. J. van Ooij, D. Zhu, M. Stacy, A. Seth, T. Mugada, J. Gandhi and P. Puomi, *Tsinghua Sci Technol*, 10 (2005) 639.

28. Z. H. Tian, H. W. Shi, F. C. Liu, S. K. Xu and E. H. Han, *Prog. Org. Coat.*, 82 (2015) 81.